

# A Multimodal fNIRS-EEG Dataset for Unilateral Limb Motor Imagery

Lufeng Feng<sup>1</sup>, Baomin Xu<sup>1</sup>, Haoran Zhang<sup>1</sup>, Bihai Lin<sup>1</sup>, Zuxuan Deng<sup>1</sup>, Sidi Tao<sup>1</sup>, Chenyu Liu<sup>2</sup>, Shifan Jia<sup>3</sup>, Li Duan<sup>1\*</sup>, and Ziyu Jia<sup>4\*</sup>

<sup>1</sup>Beijing Jiaotong University, Beijing, 100044, China

<sup>2</sup>Nanyang Technological University, 50 Nanyang Avenue, Singapore

<sup>3</sup>Simon Fraser University, Vancouver V5A 1S6, Canada

<sup>4</sup>Institute of Automation, Chinese Academy of Sciences, Beijing, 100044, China

\*Corresponding authors: Li Duan (duanli@bjtu.edu.cn) and Ziyu Jia (jia.ziyu@outlook.com)

## Abstract

Unilateral limb motor imagery (MI) plays an important role in upper-limb motor rehabilitation and precise control of external devices, and places higher demands on spatial resolution. However, most existing public datasets focus on binary- or four-class left-right limb paradigms that mainly exploit coarse hemispheric lateralization, and there is still a lack of multimodal datasets that simultaneously record EEG and fNIRS for unilateral multi-directional MI. To address this gap, we constructed MIND, a public motor imagery fNIRS-EEG dataset based on a four-class directional MI paradigm of the right upper limb. The dataset includes 64-channel EEG recordings (1000 Hz) and 51-channel fNIRS recordings (47.62 Hz) from 30 participants (12 females, 18 males; aged 19.0–25.0 years). We analyse the spatiotemporal characteristics of EEG spectral power and hemodynamic responses, and validate the potential advantages of hybrid fNIRS-EEG BCIs in terms of classification accuracy. We expect that this dataset will facilitate the evaluation and comparison of neuroimaging analysis and decoding methods.

## Background & Summary

Brain–computer interfaces (BCIs) are systems that acquire and decode brain activity signals and translate them into control commands for external devices [1]. According to the signal acquisition modality, BCIs can be divided into invasive and non-invasive types [2]. Motor imagery (MI) is one of the most importance paradigms in non-invasive BCIs [3]. With the rapid expansion of BCIs into clinical practice, rehabilitation, and human–computer interaction, the potential application scenarios of MI have become increasingly diverse, including upper-limb functional reconstruction [4, 5], daily assistive control [6] and continuous trajectory [7] guidance.

MI involves a distributed motor–somatosensory–parietal network, including the primary motor cortex (M1), primary somatosensory cortex (S1), lateral premotor cortex (PMd/PMv), supplementary motor area (SMA), and the superior parietal lobule / intraparietal sulcus (SPL/IPS) (Fig. 1(a)) [17]. Traditional MI paradigms mainly focus on binary- or four-class bilateral limb tasks that are well separated in spatial location (e.g., left vs. right hand, feet and tongue MI) [3]. These paradigms are commonly used for algorithm development and benchmarking [8]. In these tasks, class discrimination mainly relies on hemispheric lateralization differences. As shown in Fig. 1(b),

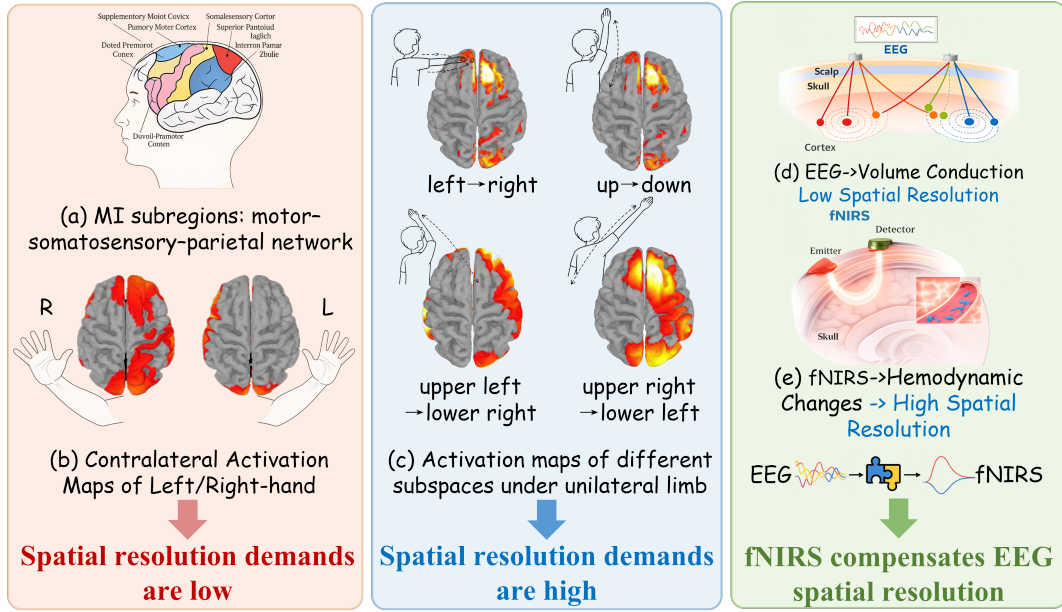


Figure 1: Motivation framework of the dataset. (a) MI subregions: motor–somatosensory–parietal network (M1/S1, PMd/PMv, SMA, and SPL/IPS). (b) Contralateral Activation Maps of Left/Right-hand. (c) Activation maps of different subspaces under unilateral limb. (d) Mechanism of EEG recording. Due to volume conduction, EEG has low spatial resolution. (e) Mechanism of fNIRS recording. fNIRS measures local  $\Delta\text{HbO}/\Delta\text{HbR}$  with higher spatial specificity. All activation maps are plotted on a common cortical surface; brighter colors indicate stronger MI-related activity.

simply identifying “which hemisphere is more active” is often sufficient to separate classes, so the requirement for spatial resolution is relatively low [15]. However, in application scenarios that require higher-dimensional control commands, such as upper-limb stroke rehabilitation [9], unilateral exoskeleton control [10], or prosthetic control [11]. Traditional MI paradigms provide limited classes and control degrees of freedom, and may not meet the need for fine and continuous upper-limb control.

Unilateral MI with multiple directions and multiple joints has a more intuitive correspondence to practical needs(e.g., upper-limb rehabilitation, and daily assistive control). Without substantially increasing cognitive load, unilateral MI can provide higher control freedom and better action separability [12, 13], and thus has become an active topic in MI-BCI research in recent years [14]. Unilateral multi-class MI typically does not show strong cross-hemisphere contrasts. Instead, class differences are reflected by subtle spatial modulations within the motor–somatosensory–parietal network of the same hemisphere. [16]. For example, in M1/PMC/SPL, representations of the hand, wrist, elbow, and shoulder are not isolated, non-overlapping “blocks” [17]. They form a proximal–distal somatotopic gradient along the precentral gyrus [18]. Different movement directions (e.g., rightward abduction vs. right-upward lifting) often manifest as small shifts of the activation centroid within this map, and as differences in coupling with parietal regions involved in spatial attention and motor planning (e.g., SPL/IPS) [19]. Fig. 1(c) illustrates local cortical differences across four unilateral tasks, suggesting that directional MI differences are finer-grained and thus impose higher demands on imaging and decoding spatial resolution.

Compared with bilateral paradigms, unilateral multi-joint and multi-direction MI depends more

on high-precision spatial information. Due to volume conduction, each scalp EEG electrode (e.g., around C3, C1, and CP3) records a weighted mixture of multiple nearby cortical sources (Fig. 1(d)), leading to low spatial resolution [20]. Therefore, relying on scalp EEG alone can cause source mixing, which averages out subtle source-level differences and limits unilateral MI decoding performance. Moreover, most existing unilateral directional multi-class datasets are EEG-only. To fill this gap, we introduce functional near-infrared spectroscopy (fNIRS), which provides higher spatial specificity. fNIRS measures local hemodynamic responses via  $\Delta\text{HbO}/\Delta\text{HbR}$ , offering a more spatially precise description of cortical activation (Fig. 1(e)) and complementary spatial information to EEG, as supported by prior studies [21]. In addition, fNIRS has relatively good cortical spatial resolution, is more robust to EMG/electrical noise artefacts, and can be recorded simultaneously with EEG without mutual interference. Compared with fMRI, fNIRS is low-cost, portable, and practical, making it suitable for wider use [37].

To compensate for the limited spatial resolution of EEG, we design a multimodal fNIRS-EEG unilateral upper-limb four-class directional motor imagery paradigm and release an open dataset, named Motor Imagery fNIRS-EEG Dataset (MIND). The MIND dataset contains EEG and fNIRS recordings from 30 participants. EEG was recorded from 64 electrodes positioned according to the international 10-20 system, and fNIRS was recorded from 51 measurement channels. Each participant completed three blocks (six sessions in total). Each session included a 60 seconds resting state and trials of two 10 seconds unilateral upper-limb MI conditions. In total, each participant performed 120 trials (30 trials per MI class), yielding 3,600 EEG and fNIRS trials across all subjects.

The dataset provides raw recordings to support flexible data analysis and benchmarking of decoding algorithms. To demonstrate data quality, we performed preliminary time-, frequency- and topography-domain analyses of the simultaneously acquired fNIRS-EEG signals. We further used standard machine-learning methods to compare single-modal and multimodal four-class decoding, confirming the advantage of multimodal fusion. We expect that the MIND dataset will facilitate the development of data-driven methods for both standalone EEG-based and hybrid fNIRS-EEG MI-BCI systems.

In existing public MI-BCI datasets, most paradigms use bilateral 2-class or 4-class MI tasks and are primarily based on single-modality EEG, such as BCI Competition IV [22,23], PhysioNet EEG-MI [24], Cho 2017 [25], OpenBMI [26], and Kaya 2018 [27], which are widely used benchmarks for algorithm development. With the shift toward practical applications, more realistic EEG datasets have been released, including cross-day settings (e.g., Cross-Session MI [28]), paradigms with interference tasks (e.g., MI under Distraction [29]), and datasets designed for stroke rehabilitation (e.g., Acute Stroke MI [30] and Lower-limb Stroke Longitudinal [31]). However, these datasets are still largely limited to bilateral paradigms or EEG-only recordings. Meanwhile, a small number of multimodal fNIRS-EEG and unilateral MI datasets have emerged. For example, Shin 2017 [32] provided a hybrid fNIRS-EEG dataset for left-/right-hand MI and mental arithmetic. OpenNeuro ds004022 [33] collected fNIRS-EEG signals during limb MI. Yi et al. [35] released an fNIRS-EEG dataset for unilateral upper-limb multi-joint MI in Scientific Data. Rong et al. [12] reported EEG decoding performance for unilateral upper-limb multi-class directional MI. In addition, some related unilateral multi-joint MI paradigms (e.g., Guo et al. [34]) have been studied but have not been released as complete public datasets. As summarized in Table 1, publicly available datasets that simultaneously satisfy the combination of unilateral upper limb, multi-class 2D directional commands, and multimodal fNIRS-EEG are still missing.

Table 1: Comparison of representative MI-BCI datasets and related studies. ✓ indicates “yes” and – indicates “no / not reported”.

Dataset / Year	fNIRS-EEG	Unilateral	Directional	Public	Notes
BCI-IV-2a (2008)	–	–	–	✓	L/R hand, foot, tongue
BBCI-IV-2b (2008)	–	–	–	✓	L/R hand
PhysioNet EEG-MI (2004)	–	–	–	✓	L/R; both fists / both feet
Cho (2017)	–	–	–	✓	L/R hand
OpenBMI (2019)	–	–	–	✓	MI / ERP / SSVEP
Kaya (2018)	–	–	–	✓	Up to 6 imagery tasks; includes 4-class MI settings
Cross-Session MI (2022)	–	–	–	✓	L/R hand
MI under Distraction (2020)	–	–	–	✓	Reach/MI with an interference task
Acute Stroke MI (2024)	–	✓	–	✓	L/R hand-grip imagery (stroke)
Lower-limb Stroke Longitudinal (2025)	–	✓	–	✓	Lower-limb gait MI (with sensory cueing/stimulation)
TU Berlin hBCI (2017)	✓	–	–	✓	L/R + MA (mental arithmetic)
OpenNeuro (2022)	✓	–	–	✓	Grasp → Twist → Reach → Lift
Guo (2024)	✓	–	–	–	L/R
Rong (2024)	–	✓	✓	–	Unilateral upper-limb 4-class MI (direction)
Yi (2025)	✓	✓	–	✓	Unilateral upper-limb multi-joint MI
Yang (2025)	–	–	–	✓	MI (L/R/feet)
<b>Proposed</b>	✓	✓	✓	✓	Unilateral upper-limb 4-class MI (direction)

## Methods

### Participants

In this study, we recruited 30 healthy, right-handed participants (18 males, 12 females; 19–25 years old) from college students. All participants had normal or corrected-to-normal vision and reported no history of neurological, psychiatric, or musculoskeletal disorders that could affect the experimental results. The study protocol was approved by the Ethics Committee. All procedures followed institutional review board (IRB) guidelines and relevant privacy regulations. Before the experiment, participants received a detailed explanation of the study purpose, procedures, and requirements, including being in good physical condition during the 24 hours before the experiment, getting sufficient sleep, avoiding alcohol and caffeine, and washing their hair in advance to ensure good signal quality. After confirming that they understood the instructions, all participants voluntarily signed written informed consent forms.

Strict environmental controls were maintained throughout the EEG and fNIRS data acquisition. We avoided strong magnetic fields in the experimental area, minimized external sensory interference such as ambient noise and light, and kept the room quiet and dim to reduce distractions. Additional measures were taken to maximise participant comfort and to reduce movement-related artefacts during recording. To minimise age-related variability and ensure consistent understanding of the tasks, all participants were university students. The recruitment procedure emphasised privacy and confidentiality, and clearly stated that participation was voluntary.

## Experimental Paradigm

The experimental paradigm was designed to elicit cortical activation patterns corresponding to different unilateral limb motor imagery (MI) tasks. Specifically, four directional movement types were included: horizontal left-to-right, vertical up-to-down, diagonal upper-left to lower-right, and diagonal upper-right to lower-left. At the beginning of each trial, participants received simultaneous visual and auditory cues. For MI trials, the visual cue was presented as a 2 seconds white instructional animation on a black background. For rest, a white fixation cross was displayed on a black background together with text indicating the duration of the upcoming rest period (Fig. 2).

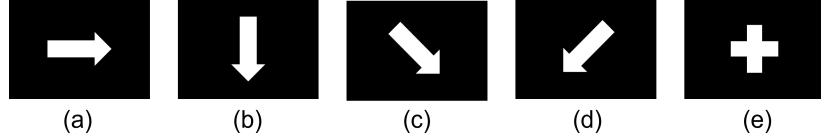


Figure 2: Representations of visual instruction to each unilateral limb task. (a) horizontal movement from left to right. (b) vertical movement from top to bottom. (c) diagonal movement from upper left to lower right. (d) diagonal movement from upper right to lower left (e) rest.

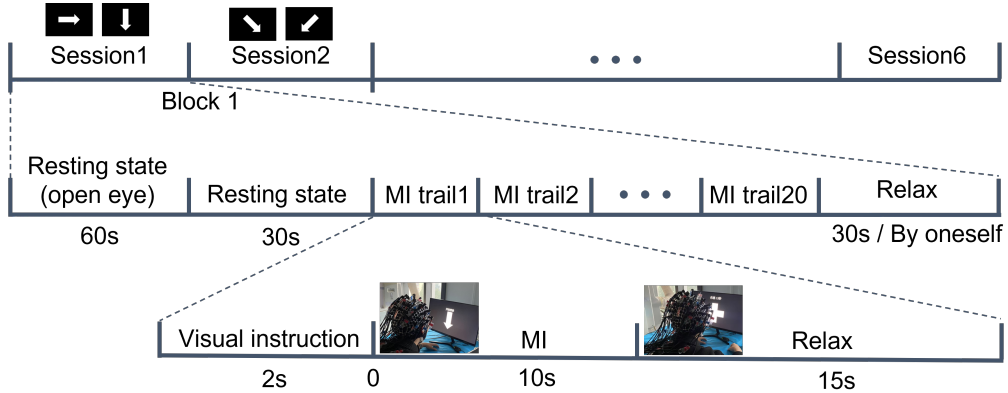


Figure 3: Experimental Paradigm of unilateral limb MI. Each subject completed three modules, with two sessions in each module, namely horizontal, vertical and two types of diagonal movements, totaling six sessions. Each session included a resting state and 20 MI sessions, making a total of 120 task sessions.

As shown in Fig. 3, each participant completed three blocks, and each block consisted of two sessions, resulting in six sessions per participant. To reduce potential bias caused by task-specific variability, horizontal and vertical MI tasks were assigned to one session type, whereas the two diagonal MI tasks were assigned to another session type. This grouping strategy was intended to improve the stability and reproducibility of neural responses across sessions.

Each block lasted 11 min and included a 60 seconds eyes-open rest, a 60 seconds eyes-closed rest, and 20 MI trials. As illustrated in Fig. 3, each trial lasted 27 seconds. The trial began with a 2 seconds visual cue, at 0 second, visual and auditory cues were presented synchronously, with a white arrow on a black background indicating the required imagery direction and the Chinese characters “开始想象 (Start imagining)”, accompanied by a short “ding” sound. This was followed by a 10 seconds MI execution period, during which participants were instructed to continuously imagine performing the cued limb movement and were encouraged to mentally repeat the movement

2–4 times within this interval. After the MI phase, a white fixation cross on a black background was shown, indicating the start of a 15 seconds inter-trial rest period. Each session contained 20 MI trials, giving a total of 120 trials per participant across the six sessions. The four MI task types (horizontal, vertical and the two diagonal directions) were each performed 30 times. To ensure data quality and minimise confounding factors, extraneous visual or auditory stimuli were strictly avoided throughout the experiment, providing a controlled and consistent sensory environment.

## Data collection and Preprocessing

## Data collection

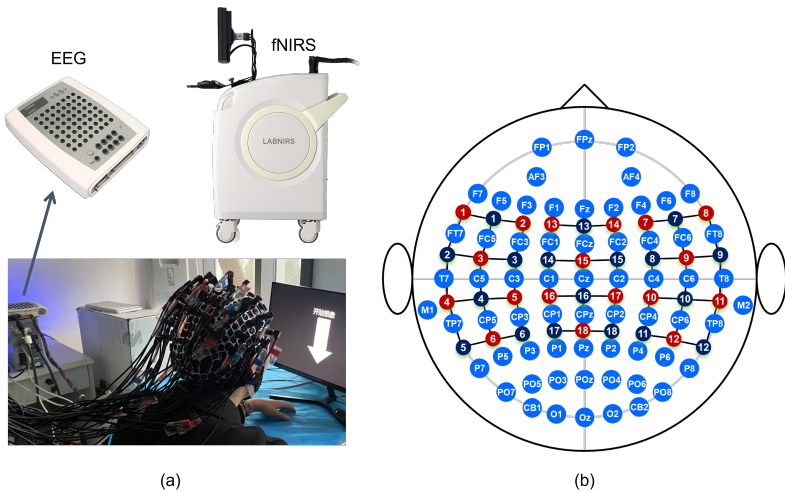


Figure 4: The instrumentation used in eeg data collection. (a) The EEG cap and signal amplifier. (b) The electrode positions on the EEG cap.

An integrated fNIRS-EEG cap and signal synchroniser developed by RSx&r was used to enable joint acquisition and precise temporal alignment of both modalities (Fig. 4(a)). The channel layout for the integrated fNIRS-EEG recording is shown in Fig. 4(b). All recordings were conducted in a controlled environment to minimise ambient light interference and movement-related artefacts, and participants were instructed to remain as still as possible throughout the experiment. The experimental paradigm was designed and implemented using E-Prime 3.0 and its development environment E-Studio [38]. Timing synchronisation between the fNIRS-EEG recording system and the experimental paradigm was achieved via digital triggers sent from E-Prime to the amplifiers, ensuring precise alignment between task events and physiological data.

EEG signals were recorded using a solid electrode cap equipped with 64 Ag/AgCl electrodes arranged according to the international 10–20 system (Neuroscan). This type of electrode cap provides high current density, strong anti-interference capability and low contact impedance. Signal acquisition was performed with a Neuroscan synAmps2 wireless amplifier, which supports real-time impedance monitoring and operates in a wireless transceiver mode (Fig. 4(a)). The reference electrode (REF) was placed over the parietal region, and the ground electrode (GND) was positioned on the forehead. EEG signals were sampled at 1000 Hz. During data collection, electrode impedance was maintained below 10 k $\Omega$  to ensure signal quality. The spatial distribution of electrodes on the EEG cap is illustrated in Fig. 4(b).

fNIRS signals were recorded using a continuous-wave LABNIRS system (Shimadzu Corp., Kyoto, Japan).

oto, Japan) to measure task-related hemodynamic responses. The device operated at three wavelengths (780, 805 and 830 nm). In total, 18 emitters and 18 detectors were used, forming 51 measurement channels; the spatial layout of these channels is shown in Fig. 4(b). Before each recording, the optical pathways were adjusted and checked to ensure that the signal quality of every channel met the manufacturer’s recommended criteria. The LABNIRS system outputs concentration changes in oxygenated, deoxygenated and total hemoglobin, and all fNIRS preprocessing was performed on these concentration time series.

In the present study, fNIRS signals were thus acquired with a 51-channel continuous-wave LABNIRS system (Fig. 4(a)). The optode arrangement followed the international 10–20 system, with source–detector pairs placed mainly over the prefrontal, parietal, temporal and sensorimotor cortices to capture movement-related hemodynamic activity. The inter-optode distance was set to 30 mm to ensure appropriate cortical penetration depth, and all optodes were secured using an elastic cap to maintain stable contact throughout the sessions. Data were sampled at 47.62 Hz and recorded continuously during the entire experiment.

## Data preprocessing

**EEG preprocessing:** EEG data were preprocessed using the MNE-Python toolbox [39] to reduce noise and improve signal quality for subsequent analyses. First, a 0.5–50 Hz band-pass filter was applied to remove slow drifts and high-frequency noise, followed by a 50 Hz notch filter to suppress power-line interference. Channels with poor signal quality were then reconstructed using spherical spline interpolation. Next, data segments corresponding to the four MI classes and the resting state were extracted: each MI segment lasted 25 seconds (5 seconds pre-cue interval, 10 seconds MI execution period, and 10 seconds post-imagery rest), and the resting segment lasted 60 seconds. A baseline window from –2 second to 0 second before cue onset was used for baseline correction to remove DC offsets. The sampling rate was subsequently reduced from 1000 Hz to 250 Hz to decrease computational load while preserving neurophysiologically relevant frequency components. To further denoise the data, we used the EEGLAB tool in MATLAB for independent component analysis (ICA) to decompose the EEG into 30 independent components. ICLabel automatic classification tool was applied with probability-based thresholds to identify and remove artefactual components (muscle activity, eye movements and channel noise). Finally, the preprocessed EEG data were exported in MATLAB-compatible *.mat* format for downstream decoding and statistical modelling.

**fNIRS preprocessing:** fNIRS data were preprocessed using the MNE-Python toolbox [39] to reduce noise and extract reliable hemoglobin concentration changes. First, a third-order Butterworth band-pass filter (0.02–0.2 Hz) was applied to the raw signals to remove slow drifts and high-frequency noise, while preserving task-related hemodynamic fluctuations. Using event markers, task-related time windows (e.g. from –5 second to 25 second around stimulus onset) were then extracted and segmented into single trials, yielding a three-dimensional data array with dimensions trial  $\times$  channel  $\times$  time. A baseline interval from –5 second to 0 second before task onset was used for baseline correction to remove slow offsets and drift. Finally, the fNIRS data were down-sampled to 10 Hz to reduce computational load while retaining physiologically meaningful information. The preprocessed HbO and HbR time series were exported in *.csv* format for subsequent analysis, providing a complete fNIRS preprocessing pipeline that ensures signal quality suitable for downstream analyses and decoding experiments.

## Data Records

The recordings have been released on a public data repository (ScienceDB) and are openly accessible. As shown in Fig. 5 and Fig. 6, the MIND dataset in the repository consists of two parts: (1) the raw data are stored in the folder *Datasetraw/*; (2) the processed data are stored in the folder *DatasetPreprocessing/*. In addition, a file named *dataset\_description.md* is provided, which summarizes all key information for reuse, including the sampling rates, the meaning of each variable/field, the task sequence, data loading instructions, and other relevant details. The entire MIND dataset is publicly available on the ScienceDB platform. The released data are licensed under the Creative Commons Attribution 4.0 International License (CC BY 4.0).

```
Dataset_raw/  # Raw data recording folder
  0926/          # Acquisition date
    EEG/          # Raw EEG data folder
      Acquisition 05.dat  # Continuous EEG data (including metadata and events)
      Acquisition 05.ceo  # Project-level metadata: experiment configuration, \\number of
      → channels, etc.
      Acquisition 05.dap  # Acquisition parameters: sampling rate, gain, etc.
      Acquisition 05.rs3  # Spatial and device configuration: electrode/sensor locations
      Acquisition 06.dat
      Acquisition 06.ceo
      Acquisition 06.dap
      Acquisition 06.rs3
      ...
      → ...          # Each .dat file contains one block group for one subject; each
      → subject has three consecutive .dat files
      fNIRS/          # Raw fNIRS data folder
        0926-001.csv  # Onset times and task labels for this block
        0926-001.txt  # Continuous fNIRS data (each subject has three consecutive .txt files)
        0926-002.csv
        0926-002.txt
        0926-003.csv
        0926-003.txt
        0926-101.csv
        0926-101.txt
        ...
        → ...          # Each subject has three consecutive .txt and .csv files: xx-001,
    → xx-002, xx-003
    ...
    0927/          # Other acquisition dates
      EEG/
      fNIRS/
      ...
    [Other dates]/  # Additional acquisition dates
    ...
    NIRS Event/    # Manually curated event labels for fNIRS
      0927/
        Subject_1_events.csv
        Subject_2_events.csv
        Subject_3_events.csv
      0928/
        ...
      1004/
      1020/
    Optical.txt     # Source{detector and channel coordinate information for fNIRS optodes
```

Figure 5: Directory structure of the raw multimodal fNIRS–EEG dataset.

This dataset contains simultaneously recorded EEG and fNIRS signals. The structure of the raw data is illustrated in Fig. 5. Data are organised by acquisition date, and for each date there are two subfolders: *EEG/* and *fNIRS/*. In the *EEG/* folder for a given date, four file types are present: *.dat*, *.ceo*, *.dap* and *.rs3*. The continuous raw EEG signals are stored in the *.dat* files. For

each participant, three consecutive *.dat*, *.ceo*, *.dap* and *.rs3* files are provided, ordered by increasing acquisition number. Each *.dat* file contains two consecutive sessions, so that each participant has three consecutive *.dat* files in total. For example, in 0926/*EEG*, the files *Acquisition05.dat*, *Acquisition06.dat* and *Acquisition07.dat* correspond to the three block groups of the first participant recorded on 26 September. The *.dat* files can be loaded using the Neuroscan reader in MNE-Python into a *Raw* object (here denoted as *data*). The *data.info* structure provides channel locations, sampling frequency, channel names and other metadata, and the event annotations encode the task structure. In the event codes, “1” denotes the eyes-open resting state, “2” denotes the eyes-closed resting state, and “4”– “7” denote the four MI tasks: left-to-right, up-to-down, upper-left to lower-right and upper-right to lower-left, respectively.

```
Dataset Preprocessing/
  └── Code/
  └── EEG/
    └── 0926/
      └── EEG/
        └── subject_01_motor_imagery_events.mat      # Preprocessed MI epochs for subject 1
        └── subject_01_resting_state_events.mat      # Preprocessed resting-state epochs for subject 1
        └── subject_02_motor_imagery_events.mat
        └── subject_02_resting_state_events.mat
        └── subject_03_motor_imagery_events.mat
        └── subject_03_resting_state_events.mat
    └── 0927/
      └── EEG/
    ...
  └── NIRS/
    └── 092601/
      └── hbo.csv                                # Subject 1 on date 0926 (date+subject index)
      └── hbr.csv                                # Hb0 epochs (trials x [51xtime] + label)
    └── 092602/
    └── 092603/
    └── 092701/
    └── 092702/
    ...
    └── 102001/
    └── 102002/                                  # Last subject (date 1020, subject index 02)
```

Figure 6: Directory structure of the Preprocessed multimodal EEG–fNIRS dataset.

In the *fNIRS/* folder for each date, two file types are provided: *.csv* and *.txt*. Files are named using the pattern *[date] – [ID]*, where *[ID]* is a three-digit code combining participant and block indices; within *[ID]*, the first digit indicates the participant index for that date, and the last digit indicates the block (session group) index. For example, 0926 – 001.csv and 0926 – 001.txt correspond to the first block of the first participant on 26 September; each participant has three such block IDs, e.g. 0926 – 001, 0926 – 002 and 0926 – 003. Each *.txt* file contains the raw fNIRS measurements (oxyHb, deoxyHb, totalHb, Abs780nm, Abs805nm and Abs830nm) together with channel information, while the corresponding *.csv* file stores the event onsets and labels. For the dates 0927, 0928, 1004 and 1020, fNIRS events were manually annotated. In these cases, the *Mark* column in the *.txt* data table denotes the time points at which the experimenter pressed the marker key. A helper function *hand\_mrk()* was used to read the *Time(sec)* values where *Mark* == 1, thereby obtaining the marker time series. Based on the experimental paradigm (fixed block durations), each marker press was converted into an accurate event time (*mrk\_time*) and assigned a task label. All derived events were then saved to *NIRSEvent/[date]/Subject\_X\_events.csv*, representing the combined events for the three blocks of participant X on that date. In addition, for the first participant on 0928, the second block was split into two files (0928 – 002\_1 and 0928 – 002\_2)

due to a temporary device interruption. We read both *.txt* segments separately and re-concatenated them after aligning to the unified event table *Subject\_1\_events.csv*. For the date 1004, the second block of the first participant was corrupted, so only the first and third blocks were retained.

Fig. 6 shows the structure of the preprocessed data. Preprocessed EEG signals are stored in MATLAB *.mat* files, whereas preprocessed fNIRS HbO and HbR time series are stored as *.csv* files. For each participant, two preprocessed EEG files and two preprocessed fNIRS files are provided. EEG files follow the naming convention *[date]/EEG/subject\_0\*/motor\_imagery\_events.mat* and *[date]/EEG/subject\_0\*/resting\_state\_events.mat*, where *0\** denotes the participant index for that date, and *motor\_imagery\_events* and *resting\_state\_events* correspond to MI and resting-state data, respectively. fNIRS files are named as *[data]0\*/hbr.csv* and *[data]0\*/hbo.csv*, where *[data]0\** encodes the participant's date and index. The preprocessed EEG *.mat* files can be directly loaded in MATLAB and are compatible with Python via *scipy.io.loadmat()*, while the fNIRS *.csv* files can be read using standard functions such as *pandas.read\_csv()*.

## Technical Validation

### EEG Data Analysis

**Time-domain analysis (ERD/ERS).** Event-related desynchronization/synchronization (ERD / ERS) was used to quantify changes in the sensorimotor rhythms that are closely related to motor imagery, focusing on the  $\alpha$  (8–12 Hz) and  $\beta$  (13–30 Hz) bands [40]. The computation proceeded as follows: (1) the EEG signals were band-pass filtered in the  $\alpha$  and  $\beta$  bands; (2) the filtered signal was squared at each sample point to obtain instantaneous power; (3) for each MI condition, power time series from all trials were summed and averaged; (4) a sliding time window was applied to obtain a smoothed power curve; (5) ERD/ERS was then expressed as

$$\text{ERD/ERS}(t) = \frac{A(t) - R}{R} \times 100\%, \quad (1)$$

where  $A(t)$  denotes the task-related power at time  $t$  and  $R$  denotes the baseline power.

**Frequency-domain analysis (ERSP).** Event-related spectral perturbation (ERSP) was used to characterise changes in spectral energy during MI [41]. ERSP is an EEG analysis method that examines how oscillatory power at different frequencies changes in response to specific events or tasks, providing a time-frequency representation relative to a baseline period, which is typically a rest or quiet state. In this study, ERSP was computed as follows: (1) preprocessed EEG data were decomposed in the time-frequency domain using the short-time Fourier transform (STFT); (2) spectral power was computed for each time-frequency point; (3) the interval preceding MI onset was used as the baseline; (4) ERSP was obtained as the average spectral energy across trials:

$$\text{ERSP}(f, t) = \frac{1}{n} \sum_{k=1}^n |F_k(f, t)|^2, \quad (2)$$

where  $F_k(f, t)$  is the complex STFT value for trial  $k$  at frequency  $f$  and time  $t$ , and  $n$  is the number of trials.

Fig. 7 shows the ERD/ERS curves of the  $\alpha$  rhythm at channels C3 and C4 for the four MI tasks in Subject 1. Around the task onset (0 s), a clear power change appears at C4, and during the 0–10 s MI period the power at C4 remains higher than that at C3. This pattern is consistent with the typical contralateral–ipsilateral effect in actual movement, where activation of the contralateral

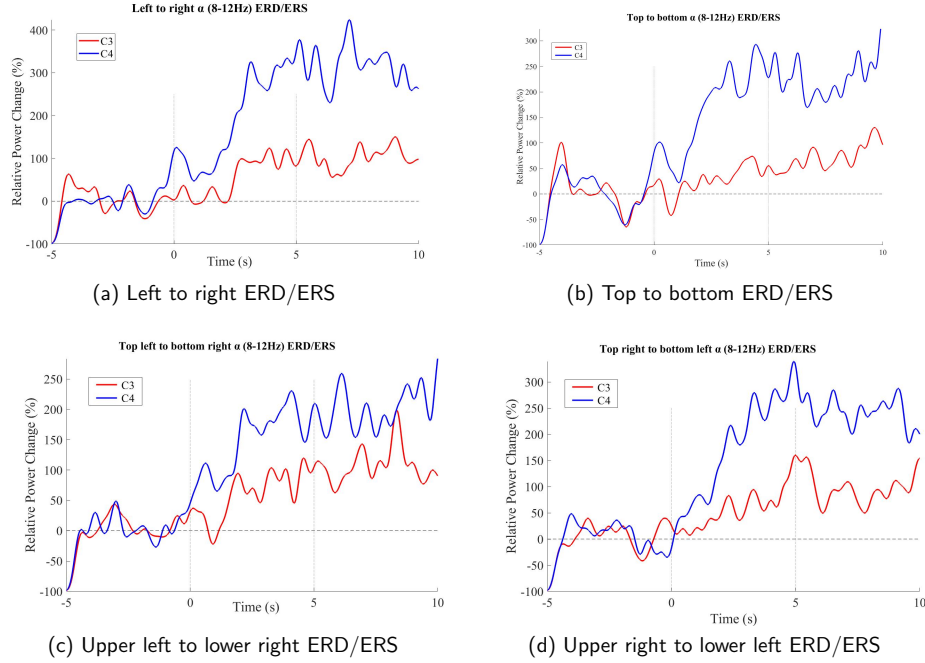


Figure 7: Four MI tasks: ERD/ERS curves of C3 and C4 in the  $\alpha$  band (8–12 Hz).

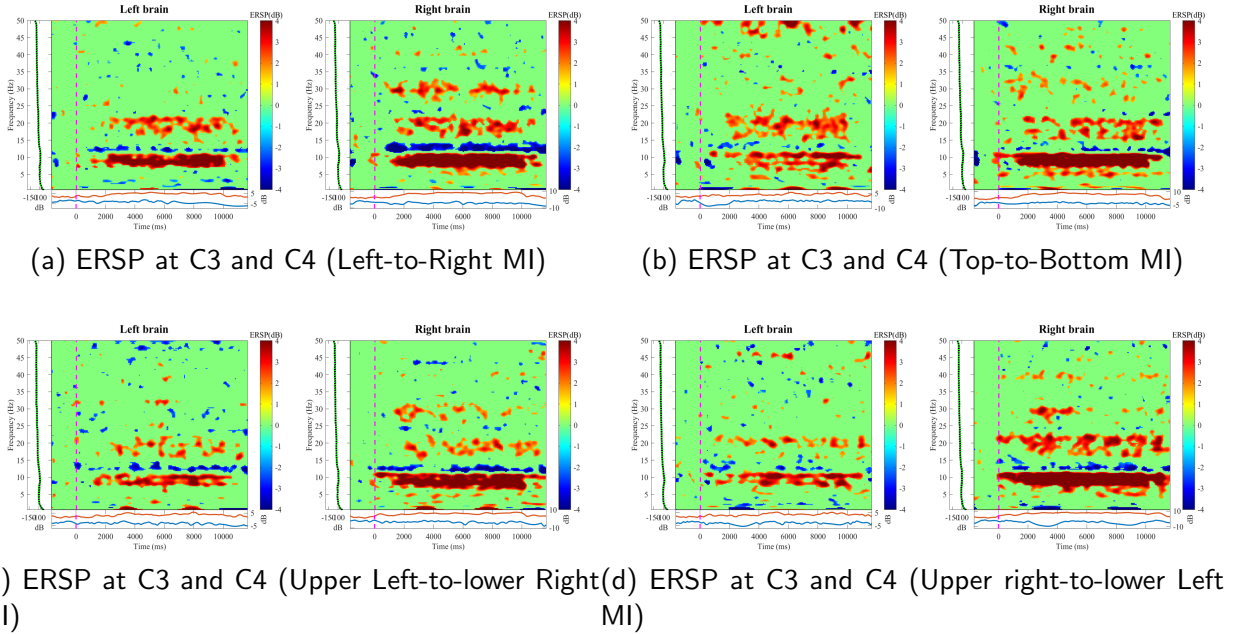


Figure 8: Average ERSP maps (8–30 Hz) over left and right sensorimotor areas (C3 and C4) during four MI tasks.

sensorimotor cortex is accompanied by  $\alpha$ -power suppression, while the ipsilateral side shows a relative power increase.

Fig. 8 shows the ERSP in the 0.5–50 Hz frequency band for four MI tasks: (a) Left-to-Right MI, (b) Top-to-Bottom MI, (c) Upper Left-to-Lower Right MI, and (d) Upper Right-to-Lower Left

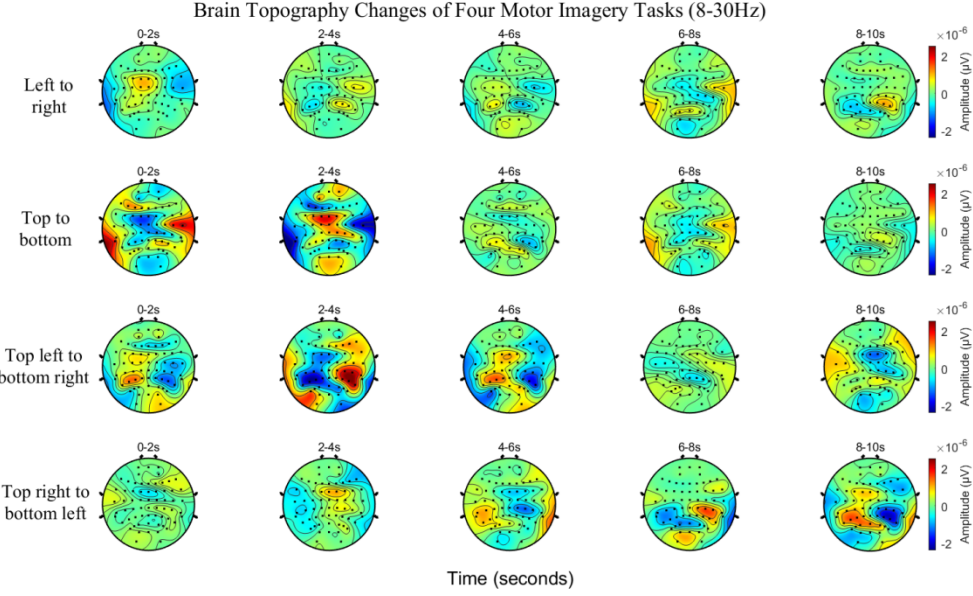


Figure 9: Topographic distribution of EEG for four directional motor imagery tasks.

MI. The figure demonstrates that after the event onset in all four tasks, the C3 channel shows significant power enhancement (red region) in the 8–12 Hz and 15–20 Hz frequency bands, while power suppression (blue region) occurs in the 12–15 Hz rhythm. Additionally, the C4 channel on the right side shows significant power enhancement (red region) in the 8–12 Hz, 15–20 Hz, and 30 Hz frequency bands, which is stronger than the left C3 channel, indicating contralateral dominance.

Fig. 9 shows the time-varying scalp topographies in the 8–30 Hz band for the four motor imagery (MI) tasks. From top to bottom, each row corresponds to one task condition: left-to-right, top-to-bottom, upper-left-to-lower-right, and upper-right-to-lower-left, respectively. Each column represents a different time window from 0–2 s to 8–10 s after cue onset. Colors indicate power changes (in  $\mu\text{V}^2$ ), with red denoting power increases and blue denoting power decreases. The maps reveal that different MI directions evoke distinct activation patterns in specific regions (especially around the central sensorimotor cortex) and show clear temporal evolution, reflecting the spatial–temporal response of cortical areas to different movement directions. A contralateral lateralization pattern can be observed in the spatial distribution, whereas within-hemisphere differences between the four tasks are subtle and cannot be reliably distinguished by visual inspection alone.

## fNIRS Data Analysis

Fig. 10 shows the event-related hemodynamic responses of Subject 1 during the four motor imagery (MI) tasks. Panels (a)–(d) depict the averaged time courses of oxygenated hemoglobin (HbO) and deoxygenated hemoglobin (HbR) for unilateral movements from left to right, top to bottom, upper-left to lower-right, and upper-right to lower-left, respectively. The horizontal axis denotes time (seconds), and the vertical axis denotes concentration ( $\mu\text{M}$ ). The results indicate that all four directional MI tasks evoke a typical hemodynamic response: HbO gradually increases and reaches a peak around 5–10 seconds after cue onset, and then slowly returns toward baseline, whereas HbR shows a slight decrease or remains relatively stable over the same time window. This pattern is consistent with classical neurovascular coupling, suggesting increased metabolic demand and local

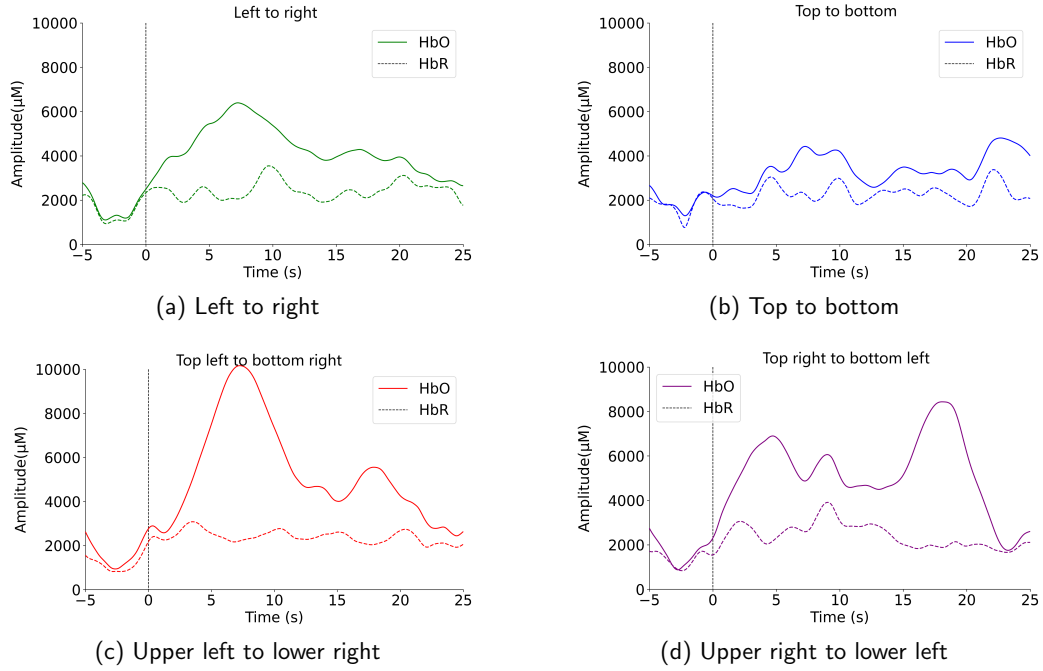


Figure 10: Average hemodynamic responses (HbO/HbR) for four directional motor imagery tasks.

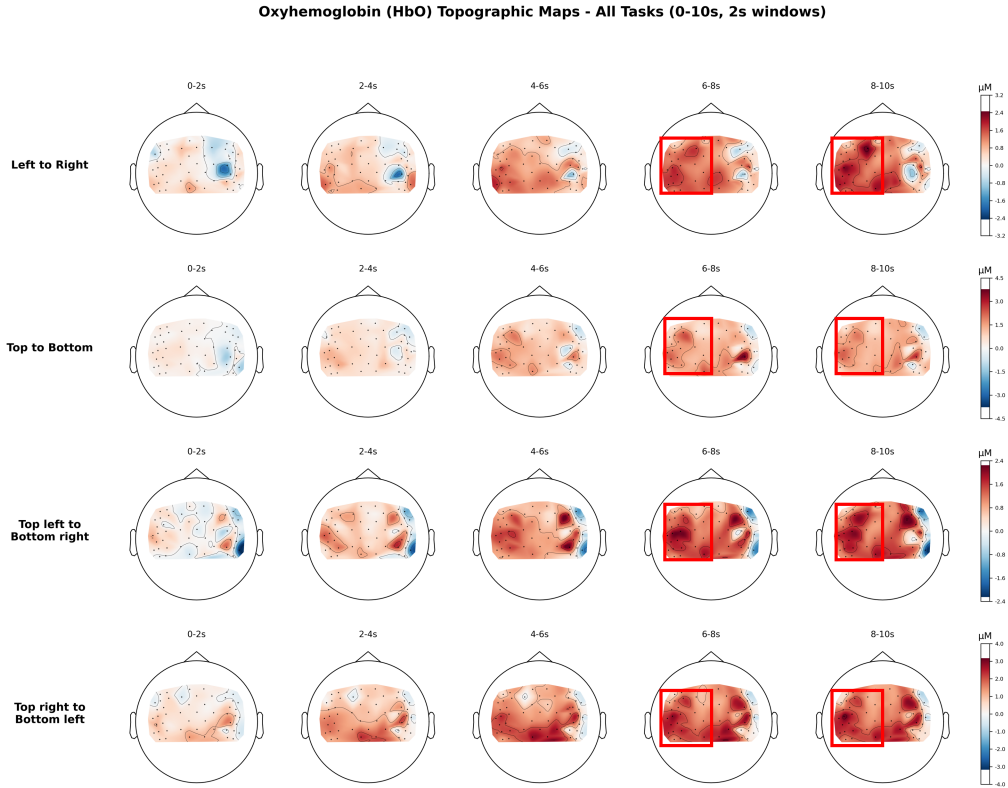


Figure 11: Topographic distribution of HbO responses for four directional motor imagery tasks.

cerebral blood flow in task-related cortical areas during MI execution. Although the four tasks share similar overall temporal profiles, they differ in peak amplitude and duration, indicating that different movement directions within the same upper limb still exhibit a certain degree of direction-specific modulation.

Fig. 11 illustrates the temporal evolution of HbO topographic maps for the four motor imagery (MI) tasks. From top to bottom, each row corresponds to the left-to-right, top-to-bottom, top-left-to-bottom-right, and top-right-to-bottom-left tasks, respectively, and from left to right each column represents a different time window from 0–2 seconds to 8–10 seconds after cue onset. Colors indicate changes in HbO concentration ( $\mu\text{M}$ ), with red denoting increases and blue denoting decreases. The red-outlined regions reach their peak response between 6 and 10 seconds. Across the four tasks, the activated areas show substantial overlap with similar centers but different boundaries, indicating that HbO in the left hemisphere increases over time within a largely shared network, while subtle spatial differences reflect direction-specific modulation.

## fNIRS–EEG classification

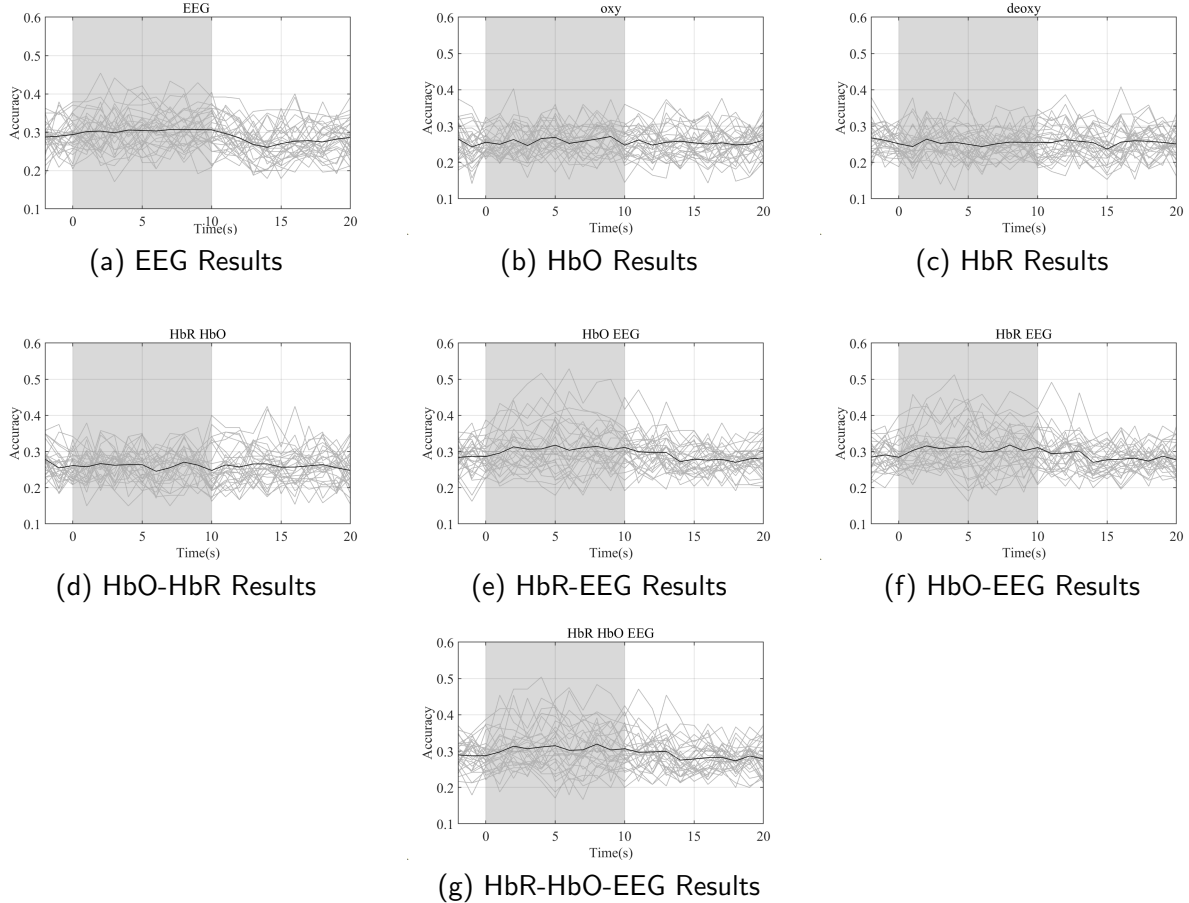


Figure 12: EEG, fNIRS, and fNIRS+EEG classification accuracies for 3 s moving time window for MI. The x-axis indicates the right edge of the moving time window. Gray lines show the individual classification accuracies while thick black lines show the average ones over whole subjects. The task starts at 0 s and finishes at 10 s. Gray shaded areas indicate task periods.

All classification analyses are performed in MATLAB R2019b using the BCI toolbox [42]. For EEG, features were extracted with a sliding-window approach (window length 3 seconds, step size 1 second) starting from -5 second and moving to 20 second relative to cue onset. Thus, the first 3 seconds window covered the interval  $[-5, -2]$  seconds, so that the time axis in the visualization started at -2 second. Filter Bank Common Spatial Pattern (FBCSP) was applied to the band-passed EEG to obtain spatially filtered signals [43]. FBCSP extends the standard Common Spatial Pattern (CSP) algorithm by splitting the signal into multiple frequency bands and performing feature selection, thereby enhancing spatial discriminability. For each window we computed the log-variance of 28 CSP components and sorted them in descending order according to their fraction of the median variance. Compared with eigenvalue-based selection, this variance-fraction criterion is more robust to outlier trials. The resulting CSP components captured the most discriminative information within each sliding window.

Sparse Linear Discriminant Analysis (sLDA) was used as the base classifier. Because sLDA is inherently binary, we adopted a one-vs-rest strategy: four independent sLDA classifiers were trained, each separating one class from the remaining three classes [32]. The final class label for each window was obtained by selecting the classifier with the highest discriminant score. To evaluate performance, we used  $10 \times 5$ -fold cross-validation and assessed classification accuracy at every sliding window. Importantly, the spatial FBCSP filters were estimated only from the training data and then applied to all windows of the corresponding test data.

For fNIRS, we used the same sliding windows as for EEG and computed two types of features for each channel: (i) the mean of  $\Delta\text{HbO}$  and  $\Delta\text{HbR}$ , and (ii) the mean slope of  $\Delta\text{HbO}$  and  $\Delta\text{HbR}$  over the window, yielding a feature vector with 51 channels and two chromophores per window. The same sLDA classifier design and cross-validation scheme as for EEG were used for fNIRS classification [32].

To assess the potential benefit of multimodal fusion, we combined the outputs (LDA projection scores) of the single-modality EEG and fNIRS classifiers into a meta-classifier feature vector. We examined all combinations (HbR+HbO, EEG+HbR, EEG+HbO, and EEG+HbR+HbO). The cross-validation procedure for the meta-classifier was identical to that used for the unimodal EEG and fNIRS classifiers.

Fig. 12 shows the time-resolved four-class MI classification accuracies for EEG, fNIRS and their fusion using 3 seconds sliding windows. The maximum mean accuracies over time reached 30.68% for EEG, 26.40% for HbR and 27.13% for HbO. After modality fusion, the maximum mean accuracies were 27.08% for HbR+HbO, 31.78% for EEG+HbO, 31.81% for EEG+HbR and 31.92% for EEG+HbR+HbO.

## Code Availability

The usage instructions for this dataset are openly available in our GitHub mirror repository (<https://github.com/usef1f/Multimodal-fNIRS-EEG-Dataset>). The folder *Code/Preprocessing/* contains preprocessing scripts for both EEG and fNIRS. For EEG preprocessing, */EEG\_process.py* and */EEGPreprocess.m* are provided. For fNIRS preprocessing, */2024\_11\_11\_snirf\_merge.ipynb* is used for automatic event labeling, and */no\_mrk.ipynb* is used for manual label refinement for sessions 0927, 0928, 1004, and 1020. The folder *Code/Plot/* includes scripts for EEG time-frequency analysis and topographic mapping, as well as fNIRS averaged hemodynamic response analysis and topographic visualization. The folder *Code/Classification/* provides unimodal and multimodal classification code based on the FBCSP+sLDA pipeline. All researchers are free to download, use, and cite these resources. We recommend reading the accompanying documentation carefully before

using the dataset, and following the original acquisition protocol and ethics statement.

## References

- [1] Vaid, S., Singh, P. & Kaur, C. EEG signal analysis for BCI interface: A review. In *Proc. Fifth Int. Conf. Adv. Comput. & Commun. Technol.* 143–147 (IEEE, 2015).
- [2] He, B., Yuan, H., Meng, J. & Gao, S. Brain–computer interfaces. In *Neural Engineering* 131–183 (Springer, 2020).
- [3] Al-Saegh, A., Dawwd, S. A. & Abdul-Jabbar, J. M. Deep learning for motor imagery EEG-based classification: A review. *Biomed. Signal Process. Control* **63**, 102172 (2021).
- [4] Mane, R., Chouhan, T. & Guan, C. BCI for stroke rehabilitation: motor and beyond. *J. Neural Eng.* **17**, 041001 (2020).
- [5] Ang, K. K. *et al.* A randomized controlled trial of EEG-based motor imagery brain–computer interface robotic rehabilitation for stroke. *Clin. EEG Neurosci.* **46**, 310–320 (2015).
- [6] Limchesing, T. J. C. *et al.* A review on recent applications of EEG-based BCI in wheelchairs and other assistive devices. In *Proc. IEEE 13th Int. Conf. Humanoid, Nanotechnol., Inf. Technol., Commun. Control, Environ. Manag.* 1–6 (IEEE, 2021).
- [7] Chen, Y.-F. *et al.* Continuous bimanual trajectory decoding of coordinated movement from EEG signals. *IEEE J. Biomed. Health Inform.* **26**, 6012–6023 (2022).
- [8] Zhang, D., Li, H. & Xie, J. MI-CAT: A transformer-based domain adaptation network for motor imagery classification. *Neural Netw.* **165**, 451–462 (2023).
- [9] Wang, A. *et al.* Rehabilitation with brain–computer interface and upper limb motor function in ischemic stroke: A randomized controlled trial. *Med* **5**, 559–569 (2024).
- [10] Tang, Z. *et al.* An upper-limb rehabilitation exoskeleton system controlled by MI recognition model with deep emphasized informative features in a VR scene. *IEEE Trans. Neural Syst. Rehabil. Eng.* **31**, 4390–4401 (2023).
- [11] Ortiz-Catalan, M. *et al.* Self-contained neuromusculoskeletal arm prostheses. *N. Engl. J. Med.* **382**, 1732–1738 (2020).
- [12] Rong, F., Yang, B. & Guan, C. Decoding multi-class motor imagery from unilateral limbs using EEG signals. *IEEE Trans. Neural Syst. Rehabil. Eng.* (2024).
- [13] Chu, Q. *et al.* Stroke-related alterations in the brain’s functional connectivity response associated with upper limb multi-joint linkage movement. *Brain Sci.* **13**, 338 (2023).
- [14] Yi, W. *et al.* A multi-modal dataset of electroencephalography and functional near-infrared spectroscopy recordings for motor imagery of multi-types of joints from unilateral upper limb. *Sci. Data* **12**, 953 (2025).
- [15] Wang, X. *et al.* Unilateral movement decoding of upper and lower limbs using magnetoencephalography. *Biomed. Signal Process. Control* **93**, 106215 (2024).
- [16] Pilgramm, S. *et al.* Motor imagery of hand actions: Decoding the content of motor imagery from brain activity in frontal and parietal motor areas. *Hum. Brain Mapp.* **37**, 81–93 (2016).
- [17] Graziano, M. S., Taylor, C. S. & Moore, T. Complex movements evoked by microstimulation of precentral cortex. *Neuron* **34**, 841–851 (2002).
- [18] Ejaz, N., Hamada, M. & Diedrichsen, J. Hand use predicts the structure of representations in sensorimotor cortex. *Nat. Neurosci.* **18**, 1034–1040 (2015).
- [19] Andersen, R. A. *et al.* Toward more versatile and intuitive cortical brain–machine interfaces. *Curr. Biol.* **24**, R885–R897 (2014).
- [20] He, B. *et al.* Electrophysiological source imaging: A noninvasive window to brain dynamics. *Annu. Rev. Biomed. Eng.* **20**, 171–196 (2018).

[21] Sun, X. *et al.* Current implications of EEG and fNIRS as functional neuroimaging techniques for motor recovery after stroke. *Med. Rev.* **4**, 492–509 (2024).

[22] Brunner, C. *et al.* BCI Competition 2008–Graz data set A. Graz Univ. Technol. (2008).

[23] Leeb, R. *et al.* BCI Competition 2008–Graz data set B. Graz Univ. Technol. (2008).

[24] Schalk, G. *et al.* BCI2000: A general-purpose brain–computer interface system. *IEEE Trans. Biomed. Eng.* **51**, 1034–1043 (2004).

[25] Cho, H. *et al.* EEG datasets for motor imagery brain–computer interface. *GigaScience* **6**, 1–8 (2017).

[26] Lee, M.-H. *et al.* EEG dataset and OpenBMI toolbox for three BCI paradigms. *GigaScience* **8**, giz002 (2019).

[27] Kaya, M. *et al.* A large electroencephalographic motor imagery dataset. *Sci. Data* **5**, 180211 (2018).

[28] Ma, J. *et al.* A large EEG dataset for studying cross-session variability in motor imagery BCI. *Sci. Data* **9**, 531 (2022).

[29] Brandl, S. & Blankertz, B. Motor imagery under distraction—an open access BCI dataset. *Front. Neurosci.* **14**, 566147 (2020).

[30] Liu, H. *et al.* An EEG motor imagery dataset for brain–computer interface in acute stroke patients. *Sci. Data* **11**, 131 (2024).

[31] Liu, Y. *et al.* Lower limb motor imagery EEG dataset based on multi-paradigm longitudinal training. *Sci. Data* **12**, 314 (2025).

[32] Shin, J. *et al.* Open access dataset for EEG+fNIRS single-trial classification. *IEEE Trans. Neural Syst. Rehabil. Eng.* **25**, 1735–1745 (2017).

[33] Lee, S. *et al.* Multimodal EEG and fNIRS biosignal acquisition during motor imagery tasks. OpenNeuro (2022).

[34] Guo, M., Feng, L., Chen, X., Li, M. & Xu, G. A novel strategy for differentiating motor imagination brain–computer interface tasks by fusing EEG and functional near-infrared spectroscopy signals. *Biomed. Signal Process. Control* **95**, 106448 (2024).

[35] Yi, W. *et al.* A multi-modal EEG–fNIRS dataset for unilateral upper limb joints. *Sci. Data* **12**, 953 (2025).

[36] Yang, B. *et al.* A multi-day high-quality EEG dataset for motor imagery BCI. *Sci. Data* **12**, 488 (2025).

[37] Codina, T., Blankertz, B. & Lühmann, A. V. Multimodal fNIRS–EEG sensor fusion. *Imaging Neurosci.* **3**, IMAG-a (2025).

[38] van Steenbergen, H., Spapé, R. & Verdonschot, M. *The E-Primer: An Introduction to Creating Psychological Experiments in E-Prime* (2019).

[39] Gramfort, A. *et al.* MEG and EEG data analysis with MNE-Python. *Front. Neurosci.* **7**, 267 (2013).

[40] Zhong, Y., Yao, L. & Wang, Y. Enhanced motor imagery decoding by calibration model-assisted with tactile ERD. *IEEE Trans. Neural Syst. Rehabil. Eng.* **31**, 4295–4305 (2023).

[41] Zhang, Z. & Koike, Y. Clustered event-related spectral perturbation feature in right hand motor imagery classification. *Front. Neurosci.* **16**, 867480 (2022).

[42] BBCI Toolbox. [https://github.com/bbci/bbci\\_public/](https://github.com/bbci/bbci_public/)

[43] Ang, K. K. *et al.* Filter bank common spatial pattern in brain–computer interface. In *Proc. IEEE Int. Joint Conf. Neural Netw.* 2390–2397 (2008).